Electronic Supplementary Material (ESI) for Chemical Communications

Supplementary Information

Access channel residues Ser315 and Asp137 in *Mycobacterium tuberculosis* catalase-peroxidase (KatG) control peroxidatic activation of the *pro*-drug isoniazid

Xiangbo Zhao,[a] Hans-Petter Hersleth,[b] Janan Zhu,[c] K. Kristoffer Andersson*[b] and Richard S. Magliozzo*[a]

[a] *Department of Chemistry, Brooklyn College and The Graduate Center of The City University of New York. 2900 Bedford Avenue, Brooklyn, NY 11210 USA Fax: 718 951 4607; Tel: 718 951 5000 X2845; E-mail: rmaglioz@brooklyn.cuny.edu*

[b] *Department of Biosciences, University of Oslo, P.O.Box 1066 Blindern, NO-0316 Oslo, Norway. . Fax: +47 2285 4726; Tel: +47 2285 6625; E-mail: k.k.andersson@ibv.uio.no*

[c] *Current address, Duke University, Durham, NC, 27705 USA*

Experimental section.

1. Overexpression of recombinant *M. tuberculosis* (*M.tb*) WT KatG and its mutant enzymes, and their purification were performed as described in previous reports;[1] the heme precursor δ-aminolevulinic acid (200 μM) was added to culture media immediately after inducing to promote formation of holo-enzyme. KatG concentration is expressed as the heme concentration based on the pyridine hemochromogen assay.

2. The rates of IN-NAD adduct generation with varying concentrations of INH were examined directly in a spectrophotometric assay according to our previous protocol [2] with minor modifications. All reactions were performed at room temp in 20mM potassium phosphate buffer (pH 7.2) containing 0.1 mM EDTA. The assay mixture contains: KatG (1 μM), NAD^+ (200 μM), Glucose Oxidase (~15 mU/mL, generating 3.0 μM/min H_2O_2), and glucose (5 mM). To monitor adduct formation, the absorbance at 326 nm was recorded for 10 min after the addition of glucose. The concentration of IN-NAD adduct was calculated according to its extinction coefficient ($\varepsilon_{326\ nm} = 6900 M^{-1}cm^{-1}$).[3, 4] The reference cuvette contained all components except NAD^+ to correct for background. The rate of adduct formation was computed from the absorbance change recorded during the first 10 min.

3. KatG[Asp137Ser] and KatG[Arg418Leu] were crystallized under conditions similar to those previously reported.[5] The crystals were grown by sitting-drop vapor diffusion with the crystallization solutions containing 100 mM sodium acetate, pH 4.6, 6% PEG 4000, and 0.17 mM n-dodecyl *β*-D-maltoside. The crystallization drop was a 1:1 mix between the crystallization solution and ~20 mg/mL KatG solution.

4. For X-ray diffraction experiments, single crystals were transferred into a cryo-solution for 10-20 seconds before being flash-frozen in liquid nitrogen in nylon loops (Hampton Research). The cryo-solutions were made by including 30% glucose as a cryoprotectant in the crystallization solutions. For the KatG[Asp137Ser] crystal, the diffraction data were collected at beam line X10SA at the SLS (Swiss-Light-Source), Villigen, Switzerland, while for the KatG[Arg418Leu] crystal, the diffraction data were collected at beamline ID29 at the ESRF (European Synchrotron Radiation Facility), Grenoble, France. Both data sets were collected at 100 K with a 6M Pilatus detector (DECTRIS, Ltd.). The diffraction data were processed and scaled with MOSFLM [6] and SCALA [7] or AIMLESS, and the space group was confirmed with POINTLESS through the CCP4 software suite [8,9]. The tetragonal structures have two KatG molecules in the asymmetric unit, and the structures were solved by molecular replacement with PHASER [10] based on the structure of WT *M.tb* KatG (PDB entry 2CCA). Refinement was performed through multiple cycles of restrained refinement in REFMAC [11] using NCS restraints, and model building and addition of water molecules in COOT.[12] No restraints were used for the $Fe{-}N_{Heme}$, $Fe{-}N_{His}$, $Fe{-}H_2O$, $C\eta2_{Trp107}{-}C\varepsilon1_{Tyr229}$ or $C\varepsilon2_{Tyr229}{-}S\delta_{Met255}$ distances. The program RADDOSE[13,14] was used to calculate the absorbed X-ray doses ($Gy = J{\cdot}kg^{-1}$) of the different crystals during crystallographic data collection. The access channel in the KatG variants was calculated with HOLLOW [15] using a 1.4 Å probe radius. The backbone Cα root mean square deviation (RMSD) values were calculated by use of PDBeFold (http://www.ebi.ac.uk) to be 0.33 Å between the WT KatG and KatG[Asp137Ser] structures and 0.35 Å between the WT KatG and KatG[Arg418Leu] structures. Structure figures were made using PyMOL.[16]

References

1. S. Chouchane, I. Lippai and R. S. Magliozzo, *Biochemistry*, 2000, **39**, 9975-9983.
2. X. Zhao, H. Yu, S. Yu, F. Wang, J. C. Sacchettini and R. S. Magliozzo, *Biochemistry*, 2006, **45**, 4131-4140.
3. B. Lei, C. J. Wei and S. C. Tu, *J. Biol. Chem.*, 2000, **275**, 2520-2526.
4. R. Rawat, A. Whitty and P. J. Tonge, *Proc. Natl. Acad. Sci. U.S.A.*, 2003, **100**, 13881-13886.
5. X. Zhao, H. Yu, S. Yu, F. Wang, J. C. Sacchettini and R. S. Magliozzo, *Biochemistry*, 2006, **45**, 4131-4140.
6. A. G. W. Leslie and H. R. Powell, in *Evolving Methods for Macromolecular Crystallography*, eds. R. J. Read and J. L. Sussman, Springer Netherlands, 2007, pp. 41-51.
7. P. Evans, *Acta Crystallogr. Sect. D Biol. Crystallogr.*, 2006, **62**, 72-82.
8. M. D. Winn, C. C. Ballard, K. D. Cowtan, E. J. Dodson, P. Emsley, P. R. Evans, R. M. Keegan, E. B. Krissinel, A. G. W. Leslie, A. McCoy, S. J. McNicholas, G. N. Murshudov, N. S. Pannu, E. A. Potterton, H. R. Powell, R. J. Read, A. Vagin and K. S. Wilson, *Acta Crystallogr. Sect. D Biol. Crystallogr.*, 2011, **67**, 235-242.
9. E. Potterton, P. Briggs, M. Turkenburg and E. Dodson, *Acta Crystallogr. Sect. D Biol. Crystallogr.*, 2003, **59**, 1131-1137.
10. A. J. McCoy, R. W. Grosse-Kunstleve, P. D. Adams, M. D. Winn, L. C. Storoni and R. J. Read, *J. Appl. Cryst.*, 2007, **40**, 658-674
11. G. N. Murshudov, P. Skubak, A. A. Lebedev, N. S. Pannu, R. A. Steiner, R. A. Nicholls, M. D. Winn, F. Long and A. A. Vagin, *Acta Crystallogr. Sect. D Biol. Crystallogr.*, 2011, **67**, 355-367.
12. P. Emsley, B. Lohkamp, W. G. Scott and K. Cowtan, *Acta Crystallogr. Sect. D Biol. Crystallogr.*, 2010, **66**, 486-501.
13. J. W. Murray, R. B. G. Ravelli and E. F. Garman, *J. Appl. Cryst.*, 2004, **37**, 513-522.
14. K. S. Paithankar and E. F. Garman, *Acta Crystallogr. Sect. D Biol. Crystallogr.*, 2010, **66**, 381-388.
15. B. Ho and F. Gruswitz, *BMC Struct. Biol.*, 2008, **8**, 49.
16. . Schrodinger, LLC, *The PyMOL Molecular Graphics System, Version 1.3r1*, (2010).

Table S1 – Crystal data, data collection and refinement statistics.

KatG	D137S	R418L
Crystal data		
Space group	$P4_22_12$	$P4_22_12$
a , *b*, *c* (Å)	150.6 / 150.6 / 157.4	150.7 / 150.7 / 157.1
$\alpha\beta\gamma$(°)	90 / 90 / 90	90 / 90 / 90
Crystal size (μm^3)	120×120×10	100×70×15
Data collection		
X-ray source	SLS-X10SA	ESRF-ID29
Wavelength (Å)	1.0000	0. 97627
Detector	Pilatus 6M	Pilatus 6M
Temperature (K)	100	100
Beam size (μm^2)	100×100	30×30
Flux (photons/sec)	$620 \cdot 10^9$	$309 \cdot 10^9$
Absorbed X-ray dose (MGy)	2.2	19.8
Resolution range (Å)	75.3-2.5 / 2.56-2.50	44.1-3.10 / 3.27-3.10
Completeness (%)*	99.9 / 100.0	99.7 / 99.8
Redundancy *	6.2 / 6.5	7.7 / 7.3
$I/\mathrm{sd}(I)$*	8.7 / 3.9	11.4 / 4.5
R_{sym} *¶	13.0 / 38.7	15.7 / 46.7
Total observations	389770	2588312
Unique reflections	62942	33364
Mosaicity	0.42	0.51
Refinement Statistics		
R_{work} (%)†	26.6	16.3
R_{free} (%)#	31.1	21.4
Mean overall isotropic B-factor ($Å^2$)	34.3	39.7
Ramachandran plot: ration in most favoured / other allowed regions / generously allowed regions (%)	88.8 / 10.9 / 0.2	87.1 /12.1 / 0.8
Estimated overall coordinate error based on R_{work}/ Maximum Likelihood (Å)	0.59 / 0.31	- / 0.28
RMSD bond (Å) / angles (°)	0.012 / 1.4	0.012 / 1.5
Solvent content (%)	56.3	56.5
Molecules per asymmetric unit	2	2
Added water molecules	82	6
Volume not occupied by model (%)	46.6	46.8
Unmodelled residues	1-24	1-23
PDB code	4C50	4C51

* The value before the backslash is for all data, and the value after the backslash is for the data in the highest resolution shell

¶ $R_{sym} = \sum|I-\langle I\rangle| / \sum I -$

† $R_{work} = \sum (|F_{obs}| - |F_{calc}|) / \sum|F_{obs}|$

R_{free} is the R_{cryst} calculated on the 5% reflections excluded for refinement.

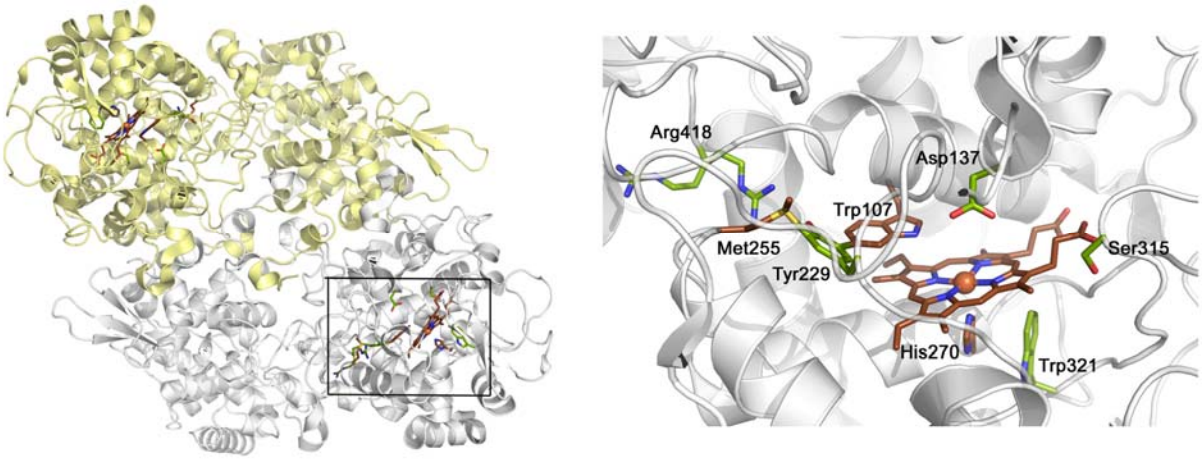

Fig. S1. Structure of the *M.tb* KatG dimer (2CCA.pdb) shown on the left. On the right, the residues mutated for this study are colored in green. The figure was generated using PyMOL.[16]

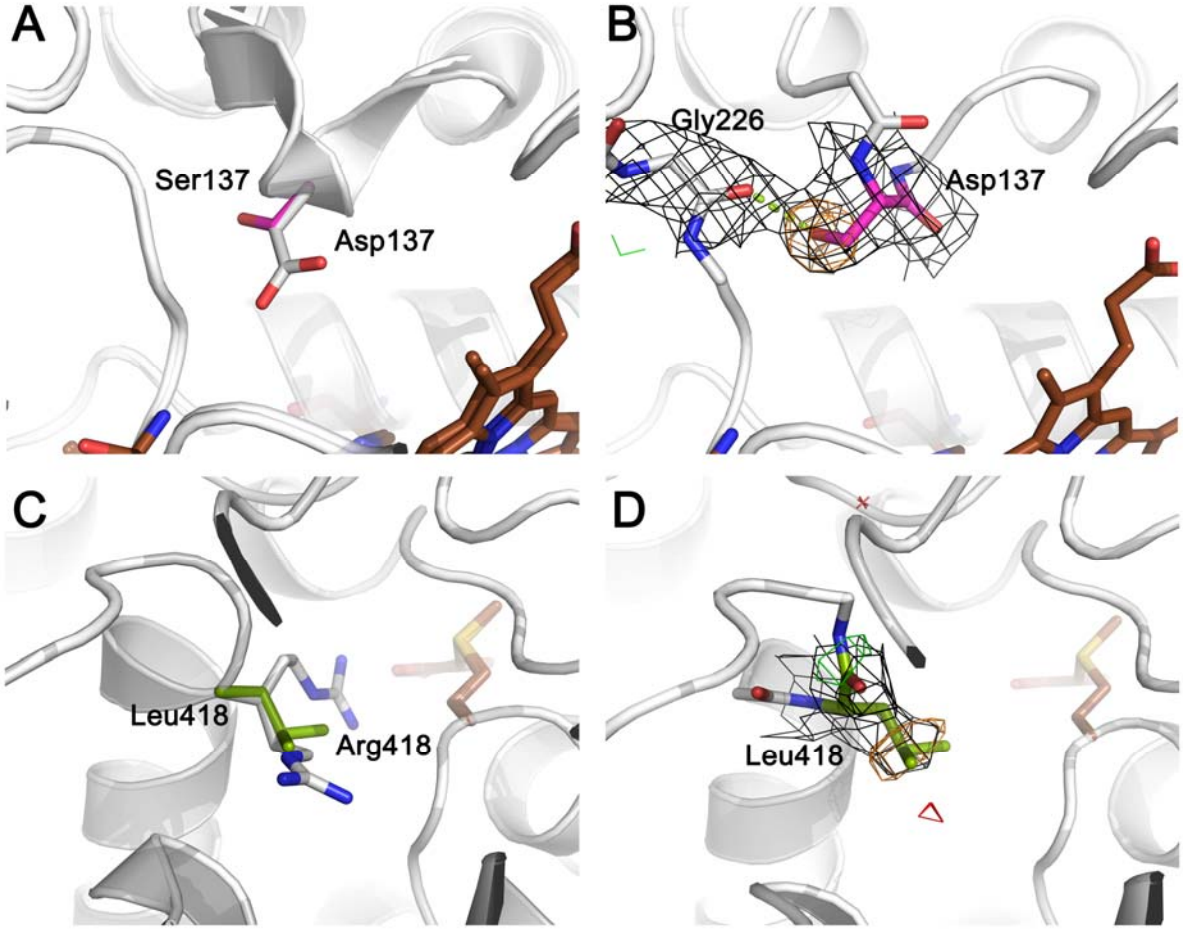

Fig. S2. Structures of the Asp137Ser and Arg418Leu mutants of *M.tb* KatG. **A.** Overlay of WT (2CCA.pdb) and Asp137Ser mutant structures; **B.** Asp137Ser mutant structure showing Ser137 and Gly226 with electron density; **C.** Overlay of WT (2CCA.pdb) and Arg418Leu mutant structures; **D.** Arg418Leu mutant structure showing Leu418 with electron density. The $2F_o$-F_c electron density maps (black) are contoured at $+1\sigma$, the F_o-F_c electron density difference maps are contoured at -3σ (red) and $+3\sigma$ (green), and the F_o-F_c OMIT-map of the mutated residues are contoured at $+4.7\sigma$ (orange). The figure was generated using PyMOL.[16]

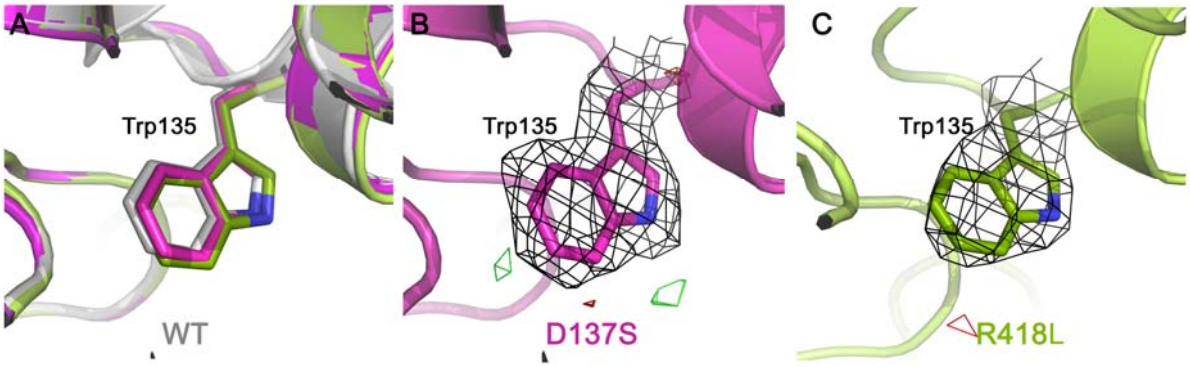

Fig. S3. Structures of *M.tb* WT KatG, KatG[Asp137Ser], and KatG[Arg418Leu] mutants showing the Trp135 residue. **A.** Overlay of WT (2CCA.pdb) and Asp137Ser and Arg418Leu structures; **B.** Asp137Ser mutant structure showing Trp135 with electron density; **C.** Arg418Leu mutant structure showing Trp135 with electron density. The $2F_o$-F_c electron density maps (black) are countered at +1σ, and the F_o-F_c electron density difference maps are contoured at -3σ (red) and +3σ (green). The figure was generated using PyMOL.[16]

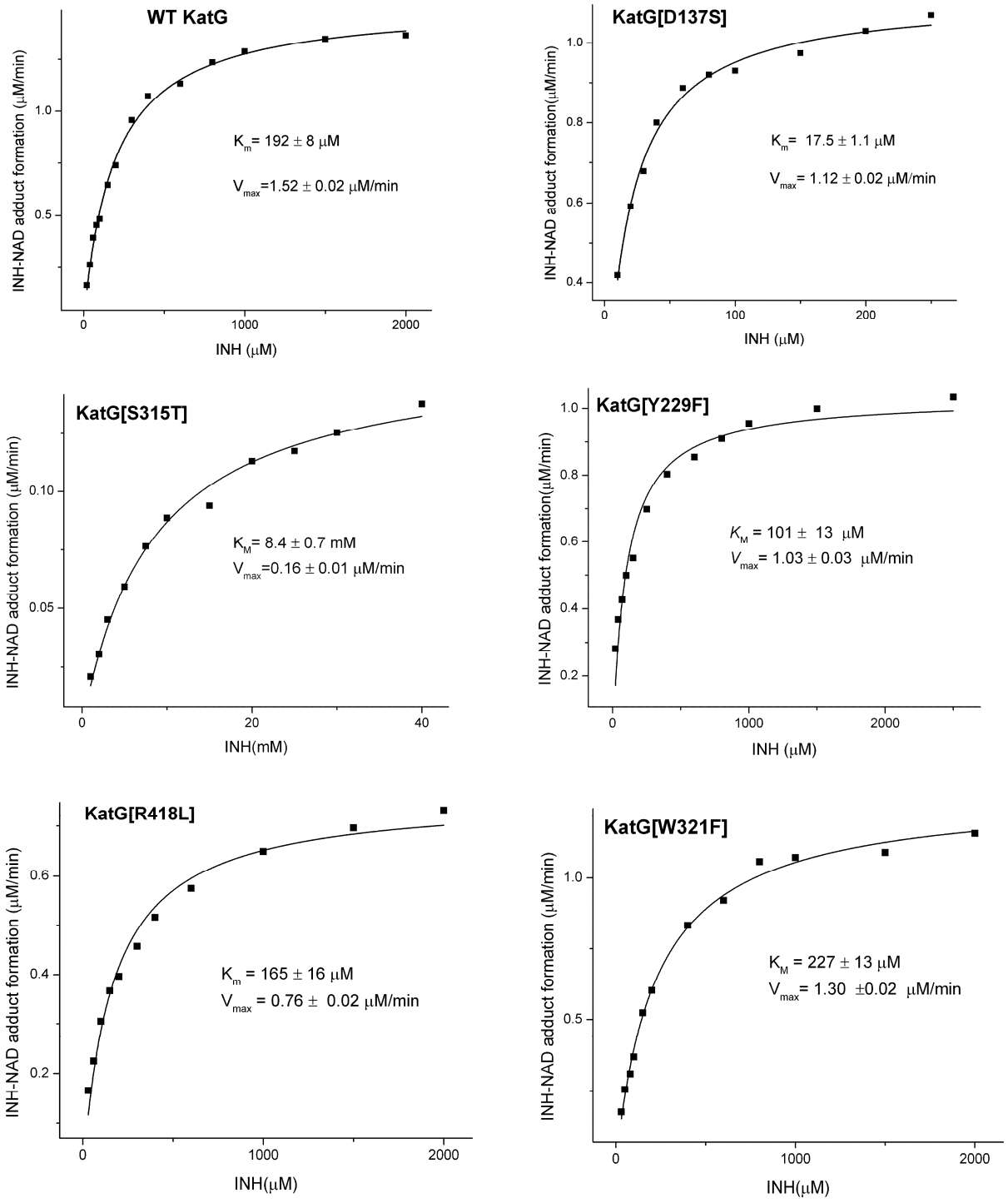

Fig. S4. Fitting of kinetics to Michaelis-Menten equation.